

THE APPLICATION OF LIGHT-ASSISTED DRYING TO THE THERMAL
STABILIZATION OF NUCLEIC ACID NANOPARTICLES

by

Phuong Anh Lam

A thesis submitted to the faculty of
The University of North Carolina at Charlotte
in partial fulfillment of the requirements
for the degree of Master of Science in
Applied Physics

Charlotte

2021

Approved by:

Dr. Susan Trammell

Dr. Donald Jacobs

Dr. Kirill Afonin

ABSTRACT

PHUONG ANH LAM. The Application of Light-Assisted Drying to the Thermal Stabilization of Nucleic Acid Nanoparticles.

(Under the direction of DR. SUSAN TRAMMELL)

Cold storage can be challenging and expensive for the transportation and storage of biologics. We are developing a new processing technique, light-assisted drying (LAD), to prepare biologics for anhydrous storage in a trehalose amorphous solid matrix. Nucleic acid nanoparticles (NANPs) are an example of new biological products that require refrigeration. DNA and RNA have emerged as building blocks for versatile biological drugs, called therapeutic nucleic acids (TNAs). NANPs have been developed to simultaneously deliver multiple TNAs and to conditionally activate TNAs and control their immunorecognition. The structural and chemical instability of NANPs over long-term storage at ambient temperatures is a challenge that may hamper broad use of this promising technology. In this work we apply the LAD technique to NANPs. NANPs suspended in a droplet of trehalose solution are irradiated with a near-IR laser to accelerate drying. As water is removed, the trehalose forms a protective matrix. The laser allows for careful control of sample temperature during processing. This is important as NANPs are thermally sensitive. In this study, RNA cubes, RNA fibers, RNA rings and DNA cubes (types of NANPs) were LAD processed and then stored for 1 month. Damage to LAD-processed NANPs was assessed after storage using gel electrophoresis and compared to unprocessed controls stored at 4°C. The thermal histories of samples were monitored during processing to determine the importance of temperature excursions on NANP viability after processing. The trehalose matrix was characterized using polarized light imaging to determine if crystallization occurred during storage, potentially damaging embedded NANPs. These studies indicate that LAD processing can stabilize NANPs for dry-state storage at room temperatures.

ACKNOWLEDGEMENTS

I would like to sincerely thank Dr. Trammell, Daniel Furr, and Riley McKeough for providing me LAD hands-on training as well as guiding me through each step of my research. I would not be able to accomplish my research without your support and guidance. To Dr. Afonin, Allison Tran, Morgan Chandler, and Damian Beasock, thank you for your collaboration, also for providing us supplies and running the gels for us.

TABLE OF CONTENTS

LIST OF TABLES	vii
LIST OF FIGURES	viii
LIST OF ABBREVIATIONS	x
CHAPTER 1: INTRODUCTION	1
1.1 Motivation	1
1.2 Anhydrous Stabilization of Biologics	1
1.3 Light-assisted Drying (LAD)	3
1.4 Nucleic Acid Nanoparticles (NANPs)	5
1.5 This Study	6
CHAPTER 2: METHODOLOGY	7
2.1 Preparation of NANPs	7
2.2 LAD Processing	7
2.3 Polarized Light Imaging	10
2.4 Gel Electrophoresis	10
CHAPTER 3: RESULTS	12
3.1 Drying Curves	12

3.2 Thermal Histories	14
3.3 Polarized Light Imaging	20
3.3.1 LAD Processed NANPs With Trehalose Added	20
3.3.2 LAD Processed RNA Rings Without Trehalose Added	23
3.4 Gel Electrophoresis	24
3.4.1 DNA Cubes, RNA Cubes and RNA Rings	24
3.4.2 RNA Fibers	26
3.4.3 Storage With and Without Trehalose in a Liquid Buffer	27
3.4.4 LAD Processing Without Trehalose	28
CHAPTER 4: DISCUSSION	30
REFERENCES	32

LIST OF TABLES

TABLE 1: EMCs of NANPs after 30 minutes and 40 minutes of LAD processing and storage	12
TABLE 2: Average crystal growth of NANPs after 1-month storage at 4°C	23
TABLE 3: Average crystal growth of NANPs after 1-month storage at room temperature	23

LIST OF FIGURES

FIGURE 1: Glass transition temperature as a function of EMC	5
FIGURE 2: LAD experimental set-up in a low relative humidity chamber	9
FIGURE 3: Polarized light imaging setup	10
FIGURE 4: Average EMC as a function of processing time for all types of NANPs	13-14
FIGURE 5: Thermal histories of NANPs during 40 minutes of LAD processing	16-17
FIGURE 6: EMCs of NANPs at maximum, minimum, and plateau temperatures	18
FIGURE 7: Temperature difference as a function of EMC	19
FIGURE 8: Thermal histories of 30-minute LAD processing for RNA rings without trehalose added	20
FIGURE 9: Unpolarized and polarized images of a DNA cube LAD processed sample pre- and post-storage at 4°C	22
FIGURE 10: Unpolarized and polarized images of an RNA cube LAD processed sample pre- and post-storage at room temperature	22
FIGURE 11: Unpolarized and polarized images of LAD processed RNA ring without trehalose	24
FIGURE 12: Native-PAGE visualizations of DNA cubes after 1 month of storage	25

FIGURE 13: Native-PAGE visualizations of RNA cubes after 1month of storage	25
FIGURE 14: Native-PAGE visualizations of RNA rings after 1month of storage	26
FIGURE 15: Native-PAGE visualizations of RNA fibers after 1month of storage	27
FIGURE 16: Native-PAGE visualizations of no-LAD RNA cubes and RNA rings after 24 days of storage	28
FIGURE 17: Native-PAGE gel of LAD processed RNA ring without trehalose and their control	29

LIST OF ABBREVIATIONS

CW	Continuous wave
DNA	Deoxyribonucleic acid
DTT	Dithiothreitol
DW%	Dry weight percent
EDTA	End moisture content
EMC	Ethylenediamine tetraacetic acid
FS	Fridge storage
FWHM	Full width at half maximum
LAD	Light assisted drying
NANPs	Nucleic acid nanoparticles
PAGE	Polyacrylamide gel electrophoresis
PCR	Polymerase chain reaction
PLI	Polarized light imaging
RNA	Ribonucleic acid
RH	Relative humidity
RT	Room temperature
UV	Ultraviolet

CHAPTER 1: INTRODUCTION

1.1 Motivation

A challenge in the development of a range of new biologics including protein-based drugs, assays, vaccines and nanomedicine products is that these items require cold-chain storage to maintain potency and/or functionality. The cold chain is a system of storing and transporting biologics at recommended temperatures from the point of manufacture to the point of use. Cold storage strategies can be challenging and expensive for the transportation of biologics and a breach in the cold chain can result in the loss of products. Further, cold chain storage can be difficult or impossible in low resource settings due to a lack of available infrastructure. For example, during the ongoing COVID-19 pandemic, everyone in the world is in need of the COVID vaccine. Two of the most common COVID vaccines, Pfizer and Moderna, need to be stored at extremely cold temperatures (-70°C and -20°C , respectively) which creates significant difficulties for vaccine distribution. Distribution of the vaccine from manufacturing facilities to local destinations has faced logistical challenges to ensure of cold-chain storage availability, efficient transportation, and on time delivery. The long-term preservation of biologics at near ambient temperatures is desirable for minimizing the cost and complexity of transportation and storage. Light-assisted drying (LAD) is a new processing technique to prepare biologics for dry-state (anhydrous) storage at elevated temperatures.

1.2 Anhydrous Stabilization of Biologics

Anhydrous preservation is storage in a dry state. Recent research has demonstrated that anhydrous preservation in a trehalose amorphous solid matrix may be an alternative to freeze drying for the preservation of biological samples. The basic idea of anhydrous preservation comes from nature. ^[1, 2] Many anhydrobiotic organisms such as baker's yeast, resurrection plants, bacteria, and microscopic animals in nature use disaccharide trehalose as a bioprotectant

to survive in their dried state. One of the interesting anhydrous micro-organisms is the tardigrade that lives around soil grains in the water film. Even in an extreme desiccated environment, tardigrades can survive for decades in a dry but viable state. After being rehydrated, the organism reverts to its active form. ^[1]

Currently, there is no standard drying technology for dehydration processing of biologics. A common strategy for anhydrous stabilization of biologics is the addition of preservative adjuvants and glass forming sugars or polymers, coupled with freeze drying, foam/vacuum drying, or spray drying. These methods all stabilize biologics in a dry state in a protective amorphous (glass) matrix composed of sugars and/or polymers. In all cases, the preservation techniques rely on removing water from sugar/polymer solutions to form the protective amorphous matrix. The techniques differ in how the removal of water is achieved. An amorphous solid restricts molecular motion to a small volume over a finite time period, which can prevent the degradation of biologics embedded in the matrix. An amorphous solid is a non-crystalline solid in which the atoms and molecules are organized such that there is no long-range order. The regular lattice of a crystalline solid can damage embedded biologics, limiting the usefulness of these solids as preservation matrices.

Freeze-drying has achieved long-term preservation at supra-zero temperatures for some biological products. ^[3-6] However, freeze-drying is a costly and complex technique. In addition, the first step of the freeze-drying process involves freezing, which induces low temperature stress, formation of ice crystals, increased ionic strength, solute concentration effects, changed pH, and phase separation. ^[7] These stresses can damage biologics, limiting the applicability of this process. Further, some biologics that are lyophilized still must be refrigerated or frozen to maintain functionality during long-term storage which does not eliminate the need for the cold chain. ^[8-11]

Foam drying produces a dried product by boiling, or foaming, the solution under reduced vapor pressure followed by rapid evaporation resulting in a solid foamy structure as the final product. Foam drying, much like freeze drying, is a complex process that requires long processing times. In addition, biologics are exposed to extreme pressure conditions during processing that can be damaging. [12, 13]

Spray drying produces a dehydrated powder by atomizing a liquid into a drying environment consisting of a heated, dry, inert gas. Spray drying exposes biologics to a hot (100°C) drying gas and aseptic processing poses a significant challenge for industrial-scale use for spray drying. [14]

Other drying techniques such as controlled humidity desiccators [15], convection drying using high flow nitrogen gas [16], and microwave drying [17] also have been utilized to dehydrate biologics in sugar solutions. However, these techniques have not proven to offer a reliable method of preservation. The resulting amorphous matrix is not spatially uniform and non-uniform distribution of water in the amorphous matrix results in destabilization of the embedded biologics.

1.3 Light-assisted drying (LAD)

We have developed a new optical processing technique, light assisted drying (LAD), to create trehalose amorphous solids for the preservation of biologics. [18, 19] LAD uses illumination with near-infrared laser light to assist in the formation of trehalose amorphous solids. Trehalose is used to form the sugar matrix because it can form an amorphous solid at room temperature and can also act as a bioprotectant, making it an attractive option as a preservation matrix for embedded biologics. [1-3] Disaccharide trehalose can act as a bioprotectant during dehydration by compensating for the loss of hydrogen bonding with water on the surface of folded proteins without changing their conformation. In this glassy state, molecular mobility within the matrix is reduced and this minimizes the degradation of biological material. [20-26] Water exhibits a strong

plasticizing effect in biological materials. [27] As an effective plasticizer, water limits the inter- and intra-molecular interactions, weakening the hydrogen bonds of biologic molecules by forming solvation shells around the molecules in the solution. The solvation shell is said to increase the distance between molecules, and lower the activation energy of segmental motion, therefore, preventing degradation of the biologics. [27]

A substantial reduction of molecular mobility is necessary to ensure an extended shelf life for anhydrous samples. To ensure this is the case, samples need to be stored below the glass transition temperature, T_g of the amorphous matrix to prevent degradation. The glass transition temperature for an amorphous trehalose solid formed by dehydration depends on the amount of water remaining in the sample after processing. The Gordon-Taylor equation can be used to predict the glass transition temperature (T_g) of trehalose-water mixtures. [21]

$$T_g = \frac{x_1 T_{g,1} + k_{GT}(1-x_1)T_{g,2}}{x_1 + k_{GT}(1-x_1)} \quad (1)$$

The glass transition temperatures of pure trehalose and pure water are given by $T_{g,1}$ and $T_{g,2}$ respectively, x_1 is the weight fraction of trehalose, and k_{GT} is an empirically determined fitting parameter of 5.2. [22] Figure 1 illustrates the glass transition temperature as a function of end moisture content, EMC. The EMC is a measure of the amount of water in a sample. The glass transition temperature increases exponentially at very low EMCs as shown in the figure. Lower moisture contents are necessary for storage at higher temperatures.

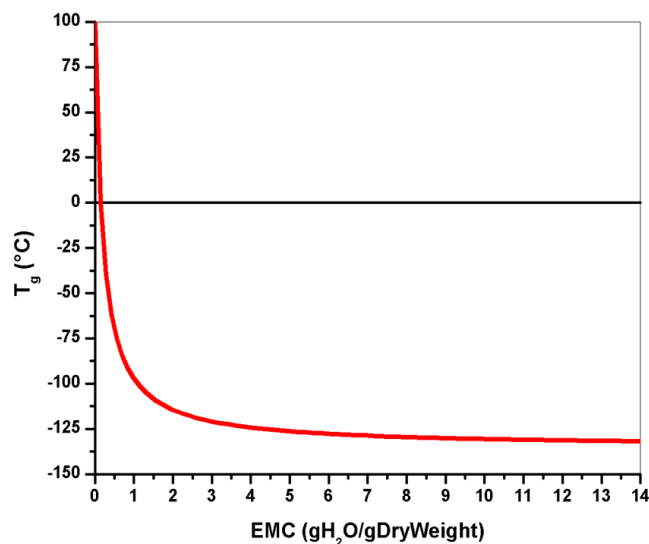


Figure 1. Glass transition temperature as a function of EMC. [15]

LAD allows for the precise deposition of energy during processing not offered by other drying techniques. The precise energy deposition yields faster and more predictable drying rates than other drying methods. It also gives control over the sample temperature during processing which is important for avoiding injury to thermally sensitive biologics. LAD processing also results in a uniform distribution of the trehalose matrix and uniform water content throughout the sample. Precise energy deposition also makes the LAD process repeatable, ensuring consistent properties of the trehalose matrix from sample to sample. This is an important consideration for the application of this drying technique in industry and for ensuring consistent storage temperatures. Further, the precise energy deposition enables rapid attainment of the desired end moisture content of the sample, which dictates sample storage temperature.

1.4 Nucleic Acid Nanoparticles (NANPs)

In this study, LAD is used to stabilize therapeutically relevant nucleic acid nanoparticles (NANPs) [28-32]. NANPs are an attractive material for diverse applications in biomedical sciences because of their programmable multi-tasking and ability to respond dynamically to environmental changes. Confirmed practical applications of NANPs include *in vivo* imaging and

therapeutic agents with regulated delivery of RNAi inducers (siRNAs and miRNAs), aptamers, ribozymes, proteins, and small molecules. [33-39] Currently, the standard for stabilization and storage of NANPs after synthesis is refrigeration in a buffer solution – cold chain storage. [40]

1.5 This Study

In this study, RNA cubes [41-45], RNA fibers [46-49], RNA rings [50-55] and DNA cubes [41-45] (four types of NANPs) were LAD processed and then stored at either room temperature (20°C) or 4°C for 1 month. We present drying curves and thermal histories that allow for the determination of appropriate LAD processing parameters and polarized light imaging (PLI) to access the quality of the trehalose matrix. Damage to LAD-processed RNA cubes was assessed after storage using gel electrophoresis. These preliminary studies indicate that LAD processing can stabilize these NANPs for dry-state storage at room temperatures.

CHAPTER 2: METHODOLOGY

2.1 Preparation of NANPs

The DNA templates for individual RNA strands were amplified via PCR with MyTaq™ Mix (Bioline). PCR products were purified with the DNA Clean and Concentrator™ kit (Zymo Research). Production of the RNA was completed via in vitro transcription starting with incubation of the DNA templates at 37°C for 3.5 hours with T7 RNA polymerase (Promega), 80 mM HEPES-KOH (pH 7.5), 2.5 mM spermidine, 50 mM DTT, 25 mM MgCl₂, and 5 mM of each rNTP. To stop the reaction, samples were incubated with RQ1 RNase-free DNase for an additional 30 minutes and then purified using denaturing 8 M urea polyacrylamide gel electrophoresis (PAGE, 15%). After visualizing the bands under UV light, they were cut out, and eluted overnight in a crush and soak buffer (300 mM NaCl, 89 mM tris-borate (pH 8.2), 2 mM EDTA). For precipitation of the RNAs, the elution was first mixed with 2.5 volumes of 100% EtOH, incubated at -20°C, centrifuged to remove supernatant, and the pellet was rinsed with 90% ethanol, vacuum dried, and dissolved in double-deionized water (17.8 MΩ·cm). Six-stranded NANPs were assembled at 0.5 μM final concentration by mixing all six RNA strands in equimolar concentrations along with doubled deionized water and assembly buffer in one-pot thermal annealing. For that, samples were heated to 95°C for 2 minutes, mixed with assembly buffer (89 mM tris-borate (pH 8.2), 2 mM MgCl₂, 50 mM KCl), and incubated at 45°C for 30 minutes. All samples were stored at 4°C after preparation.

2.2 LAD Processing

A schematic of the LAD processing system is shown in Figure 2. An IPG Photonics continuous wave (CW) ytterbium fiber laser at 1064 nm (YLR-5-1064) was used for LAD processing (maximum power output of 5 W). The laser has a factory collimated Gaussian beam with a FWHM spot size of 4.5 mm which was measured using a Beam Track 10A-PPS thermal

sensor (Ophir Photonics). A FLIR SC655 mid-IR camera was used to record the temperature of samples during processing. All studies were performed in a humidity-controlled environment that was kept at approximately 11% RH. This was achieved by pumping dry air into a chamber containing the experimental setup and monitoring the RH with a temperature and RH logger (ONSET UX100-011). Maintaining a low relative humidity expedited the drying process.

Samples consisted of 10 μL droplets of NANPs (concentration 0.25 μM) suspended in a drying solution (DS). The DS consisted of 0.2 M disaccharide trehalose in 0.33 x phosphate buffer solution (PBS). For each test, a 10 μL droplet of the NANP/drying solution was deposited onto an 18 mm diameter borosilicate glass coverslip (Fisher brand 12-546) substrate. The glass coverslips allow for easy recovery and rehydration of the NANPs after LAD processing. The initial mass of the sample was determined gravimetrically using a 0.01 mg readability balance (RADWAG AS 82/220.R2). RNA filaments (N=6), RNA rings (N=6), and RNA cubes (N=6), were processed for 40 minutes at 5 W (26.9 W/cm²), and the DNA cubes (N=6) were processed for 40 minutes at 4 W (21.5 W/cm²). DNA cubes were processed at a lower power because higher powers caused thermal damage. The temperature of the sample was monitored during processing using the thermal camera. The maximum temperatures reached during processing for the RNA filaments, RNA rings, RNA cubes, and DNA cubes were 35.4 ± 0.8 °C, 35.8 ± 0.2 °C, 35.8 ± 0.6 °C, and 31.3 ± 1.1 °C, respectively. After irradiation, the sample was removed from the humidity chamber and immediately massed again. End moisture content (EMC), which is a measure of the amount of water relative to the dry mass of a sample was calculated using Equation 2:

$$EMC = \frac{m_f - m_s - m_{dw}}{m_{dw}} \quad (2)$$

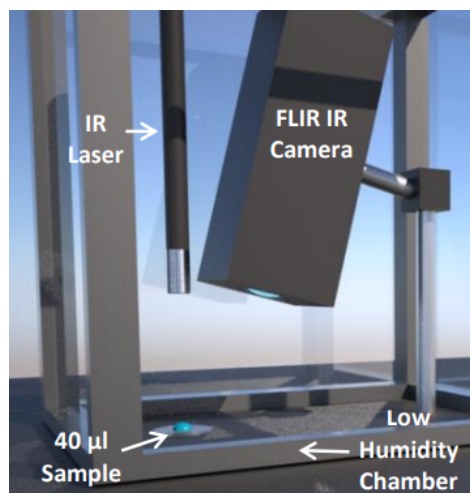


Figure 2. LAD experimental set-up in a low relative humidity chamber. ^[18]

where m_f is the mass of the final sample including the mass of the substrate, m_s is the mass of the substrate, and m_{dw} is the measured dry weight of the initial sample. The dry weight was calculated by multiplying the initial mass of the sample by the percent dry weight (%DW) which was determined via bake-out method. The %DW is dominated by trehalose and components of buffer solutions, therefore is the same for all types of NANP. The average %DW of all the NANPs is $5.9\% \pm 0.2\%$. After LAD processing, samples were stored individually in small volume containers inside moisture barrier bags (ULine) for 1 month. The RH inside the bags was 10.5 ± 0.5 RH (measured with a RH probe, HH314A, Omega). Three samples for each type of NANP were stored at 4°C and three samples were stored at room temperature (approximately 20°C).

In addition to these experiments, studies were also performed to explore the stability of RNA rings without trehalose added to the buffer solution prior to LAD processing. Small droplet samples containing RNA rings ($N=6$) in the storage buffer (no trehalose) were processed at 5 W for 30 minutes in the humidity chamber. The maximum temperature reached during LAD processing was $35.0 \pm 0.4^\circ\text{C}$.

2.3 Polarized Light Imaging

To investigate crystal growth in the stored samples, polarized light imaging (PLI) was used. The PLI experimental set-up (Figure 3) consisted of a white light fiber optic illuminator (41720, Cole Palmer), two linear polarizers (LPVISE050-A, Thorlabs), with the second polarizer acting as an analyzer, and a digital camera (Nikon D100) aligned in the vertical direction. The camera was equipped with a Nikon 28-105 mm f/3.5-4.5 lens and manually focused on the image plane. The spatial resolution of the set-up was 10 $\mu\text{m}/\text{pixel}$. Immediately after processing, samples were placed on a glass microscope slide in between the polarizers and imaged from above. Two images were taken: the first with the analyzer oriented at 0° to the polarizer and the second with the analyzer oriented at 90° to the polarizer. For each sample, images were taken immediately after processing and after storage.

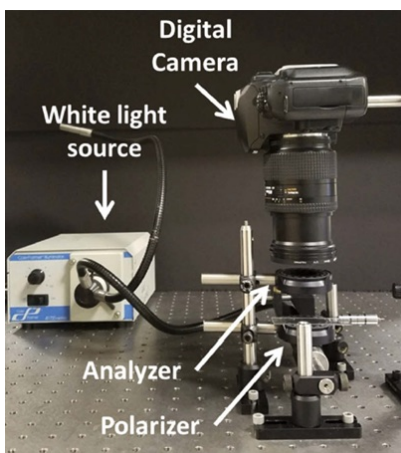


Figure 3. Polarized light imaging setup. Samples were placed between the polarizer and analyzer.

[19]

2.4 Gel Electrophoresis

Structures of assembled NANPs were verified on non-denaturing native polyacrylamide gels (native-PAGE, 8%, 37.5:1) immediately after initial assembly, after LAD processing, and after storage. Samples were rehydrated by first pipetting water (10 μL) directly onto the center of

the dried droplet and then mixing with the pipette tip. After 1-2 minutes, the solution was transferred into an Eppendorf tube. These tubes were left on ice or in the cold room (4°C) until used. The gels were run in a Mini-PROTEAN Tetra system (Bio-Rad) with running buffer (89 mM tris-borate (pH 8.2), 2 mM MgCl₂) for 30 minutes at 300 V in a 4°C cold room. Afterwards, the gels were stained with ethidium bromide for 5 minutes and washed with water. Gel imaging was completed using a ChemiDoc MP system (Bio-Rad).

CHAPTER 3: RESULTS

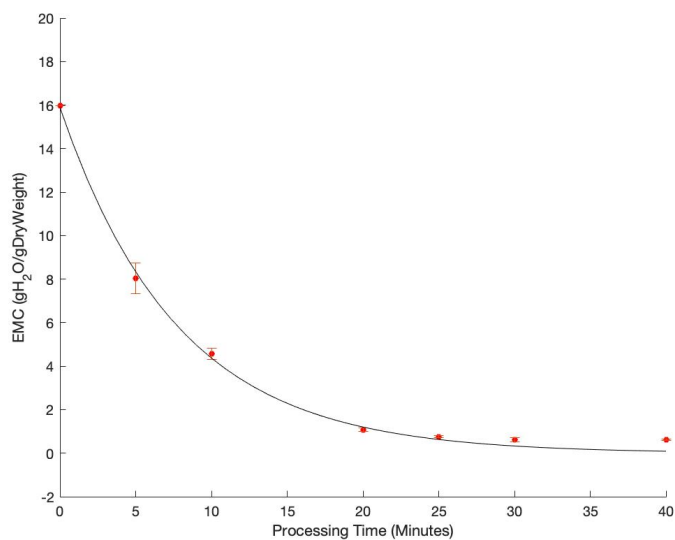
3.1 Drying Curves

Figure 4 shows the drying curves of the four types of NANPs (RNA fibers, RNA cubes, RNA rings and DNA cubes; N = 6 for each type of particle). Drying curves show how the EMC of a sample changes with processing time. Measurements of EMC were taken at processing times of 0, 5, 10, 20, 25, 30, and 40 minutes. The EMC decreases approximately exponentially as the processing time increases, indicating that the majority of sample drying occurs during the early stages of the LAD process. The EMC reaches a plateau at approximately 30 minutes and little change in the EMC is seen between 30-40 minutes of processing. The average EMC of samples after 30 and 40 minutes of processing are given in Table 1. There is no significant change in the EMC between 30-40 minutes. This suggests that a processing time of 30 minutes is sufficient to achieve low EMCs for the 10 μ l samples used in this study. Table 1 also provides the average EMC of 40 minutes of processing after 1-month storage in a low humidity environment in comparison with the average EMC right after 40 minutes LAD processing. No significant change is observed before and after storage.

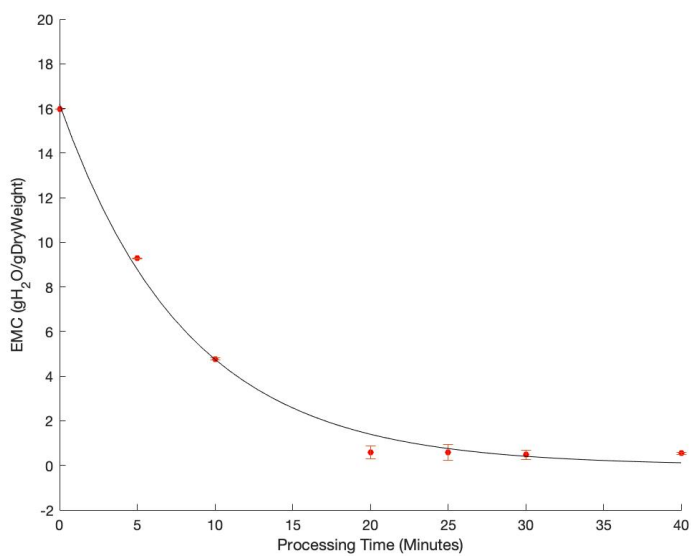
Table 1. EMCs of NANPs after 30 minutes and 40 minutes of LAD processing and storage.

Type of NANPs	Average EMC (gH ₂ O/gDryWeight)		
	30 minutes of LAD processing	40 minutes of LAD processing	40-minute-LAD processed NANPs after 1-month storage
RNA cubes	0.63 \pm 0.09	0.62 \pm 0.03	0.54 \pm 0.07
RNA fibers	0.5 \pm 0.2	0.54 \pm 0.04	0.59 \pm 0.05
RNA rings	0.69 \pm 0.06	0.85 \pm 0.04	0.88 \pm 0.05
DNA cubes	0.49 \pm 0.03	0.51 \pm 0.03	0.50 \pm 0.03

The DNA cube particles were processed at a lower laser power of 4W to prevent thermal damage to these particles. Again, no significant difference between processing times of 30 to 40 minutes are noted.

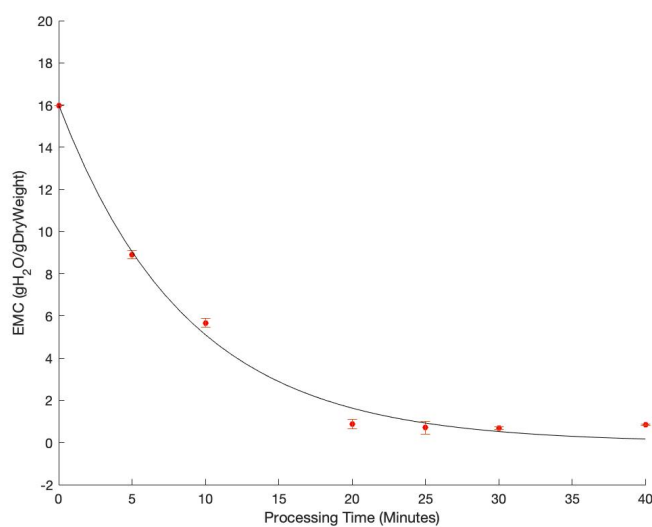


(a) RNA cubes

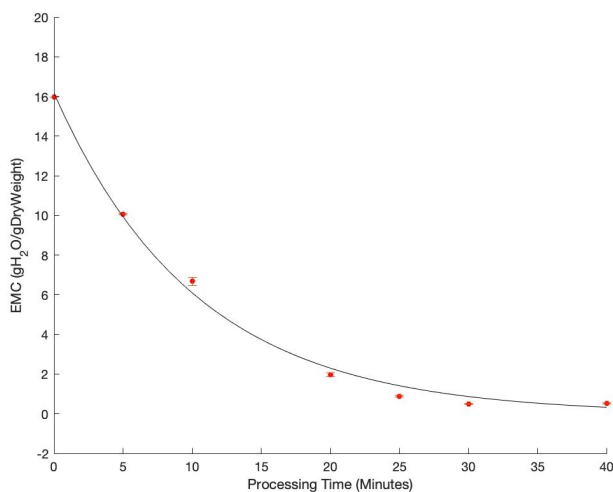


(b) RNA fibers

Figure 4. Average EMC as a function of processing time for all types of NANPs.



(c) RNA rings



(d) DNA cubes

Figure 4. (continued)

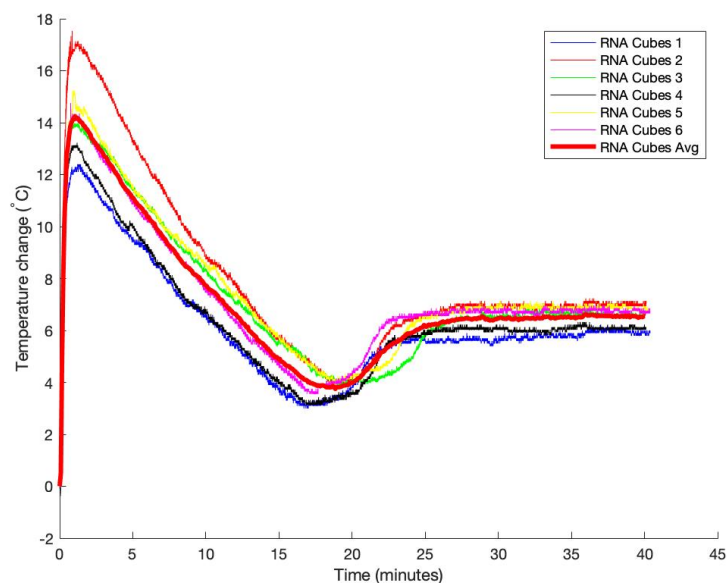
3.2 Thermal Histories

Figure 5 shows the thermal histories of RNA cubes (a), RNA fibers (b), RNA rings (c), and DNA cubes (d) (N=6 for each) and the average curves for all samples processed for 40 minutes. All of these NANPs were suspended in the trehalose buffer. All graphs show the change

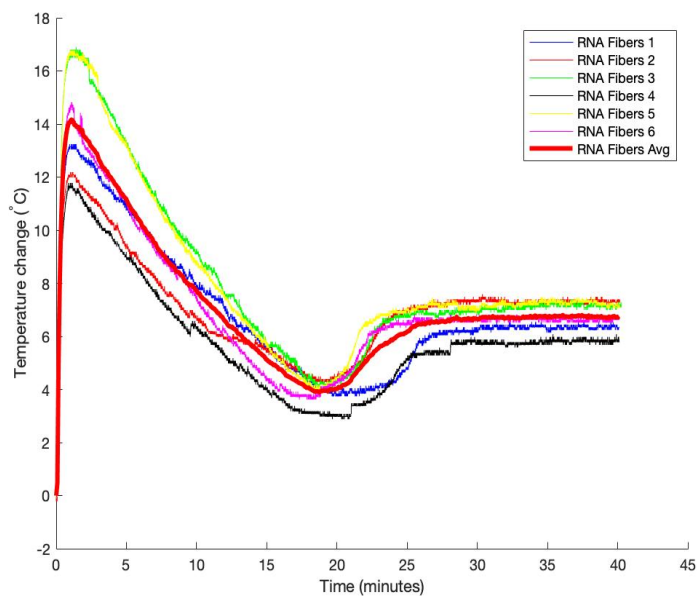
in the droplet temperature compared to the initial droplet temperature as a function of time. All RNA nanoparticles were processed at 5 W; therefore, their thermal curves are similar. Slight variations in the sample temperatures were seen for the RNA NANPs leading to slightly different changes in the temperature during processing. These small differences are likely due to fluctuations in the ambient temperature in the processing environment. The peak temperature for DNA cubes was lower than the peak temperature for all of the RNA NANPs. The DNA cubes were processed at lower laser power than the other NANPs because these NANPs have a lower melting temperature than the RNA NANPs. The lower laser means that less energy is delivered to the droplet per second. As expected, the maximum sample temperature is lower for the DNA cubes. However, the change in the temperature of the samples was similar to that seen for the RNA NANPs.

The overall shape of the thermal history is the same for all types of NANPs processed. The initial rise in the temperature is the result of laser heating of the water in the sample. A maximum temperature is reached during the first minute of processing. After this peak in temperature, evaporative cooling reduces the sample temperature, indicating that LAD is effectively removing water from the sample. Near 20 minutes, the temperature reaches a minimum value and then again starts to increase. By 30 minutes, the temperature in the sample plateaus. On this plateau, the heating and cooling are balanced resulting in a stabilization of sample temperature. This plateau seems to mark the end of significant, rapid evaporation of water from the sample. This is consistent with the EMCs seen at 30 and 40 minutes. There was no significant decline in the water content between these processing times. A higher peak temperature results in the sample temperature reaching the plateau more quickly. This is consistent with the idea that at a higher temperature, evaporation will drive water out of the

sample more quickly. Meaning that the sample will reach the end of significant evaporative cooling (the plateau) faster.

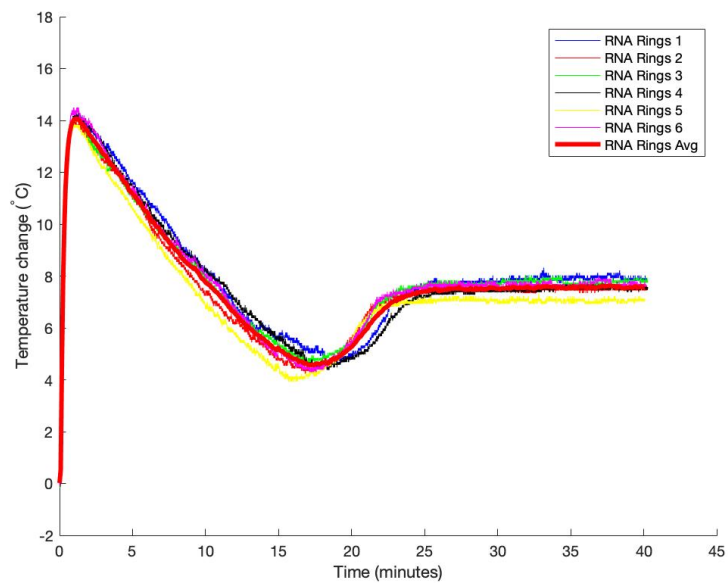


(a) RNA cubes

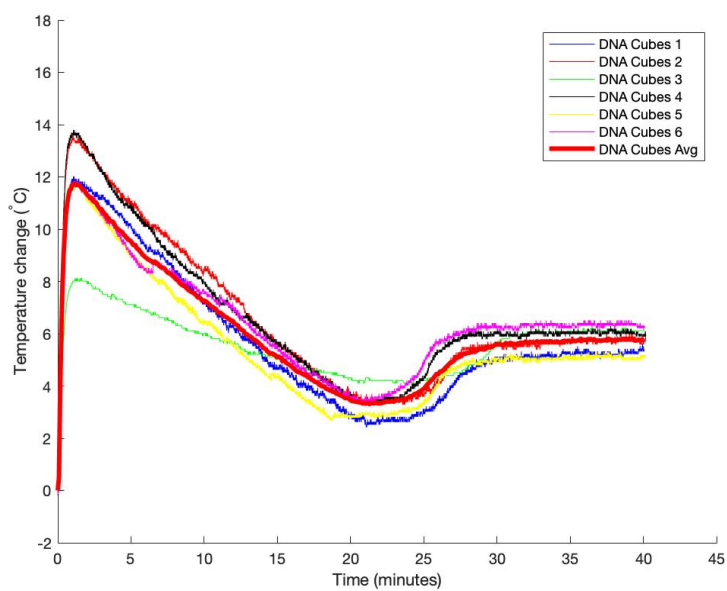


(b) RNA fibers

Figure 5. Thermal histories of NANPs during 40 minutes of LAD processing.



(c) RNA rings



(d) DNA cubes

Figure 5. (continued)

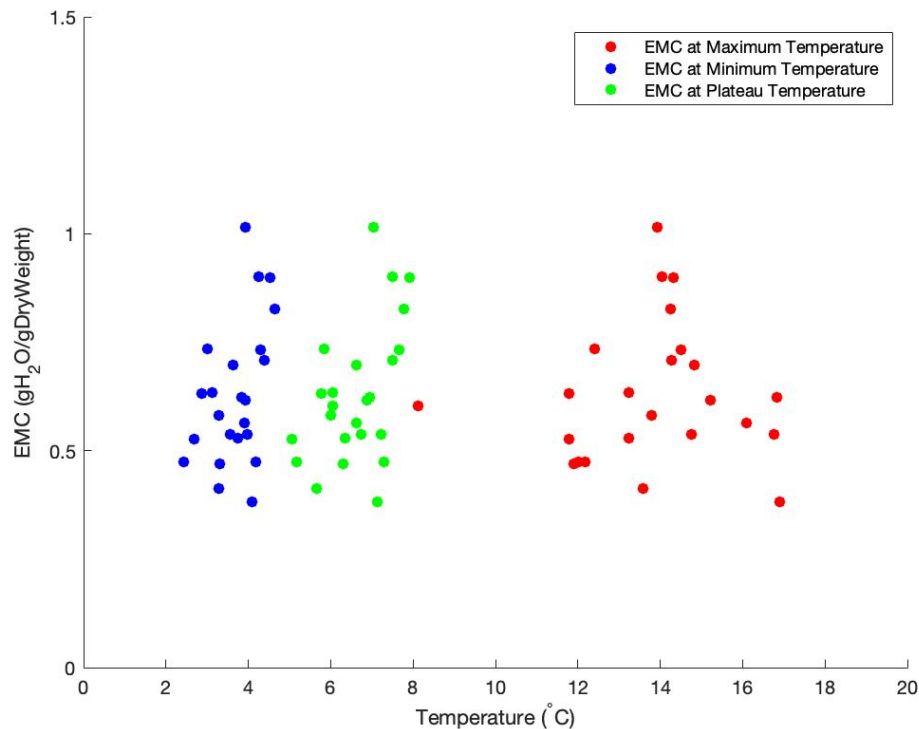


Figure 6. EMCs of NANPs at maximum, minimum, and plateau temperatures.

Figure 6 shows EMC vs. the peak, minimum, and plateau temperatures reached by the samples during LAD processing. There is little/no correlation between EMC and peak/minimum/plateau temperature. Figure 7 shows how EMC changes relative to the difference between the maxima and minima temperatures during processing. It does not show any correlation between the EMC and these temperature differences. These results suggest that the final EMC does not depend on the peak temperature as long as samples are processed until they reach the temperature plateau.

These results demonstrate that the thermal history can be used to determine the processing time that will maximize the amount of water removal from the sample during LAD processing. In previous studies, the drying curve was used to determine the optimal processing time. The thermal history is easier to acquire than the drying curve and offers a valuable tool for determining processing parameters for samples.

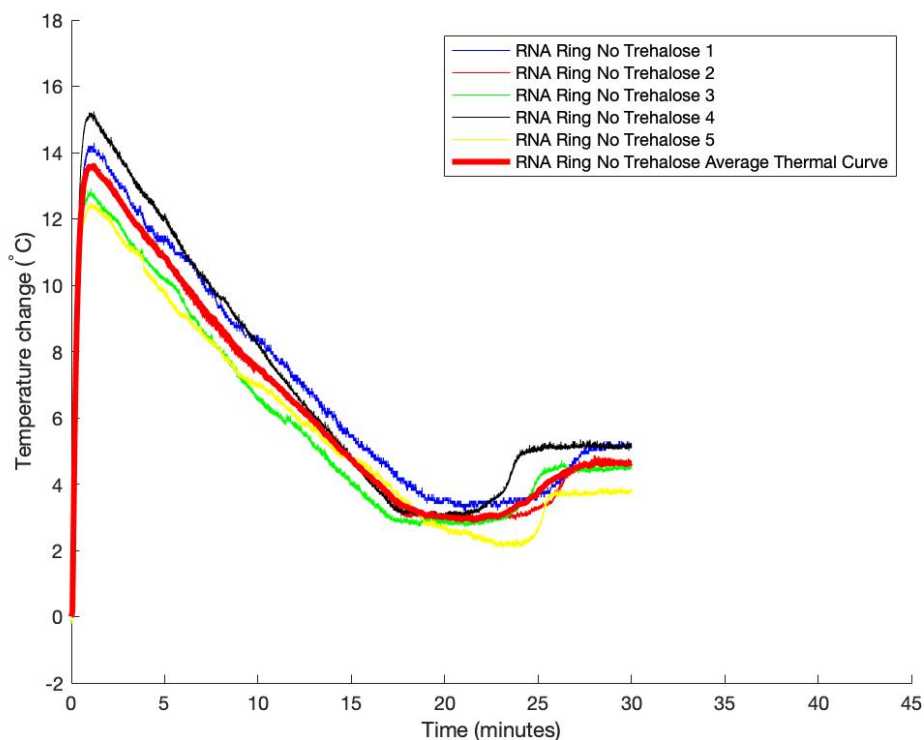


Figure 8. Thermal histories of 30-minute LAD processing for RNA rings without trehalose added.

3.3 Polarized Light Imaging

3.3.1 LAD Processed NANPs With Trehalose Added

Polarized light imaging (PLI) was used to investigate the stability of the trehalose matrix against crystallization immediately after LAD processing and after storage. As polarized light travels through the amorphous trehalose matrix, the plane of polarization of the light remains constant and the light cannot propagate through the crossed-polarizer. Any crystalline inclusions in the matrix are birefringent and will rotate the plane of polarization. If the plane of polarization changes, the light can travel through the crossed-polarizer and this area will appear as a bright spot in crossed-polarizer images.

The PLI for all NANPs is similar. Figure 9 shows the PLI of DNA cubes immediately after processing and after 1-month storage in a humidity bag at 4 °C. Figure 10 shows PLI for RNA cubes after processing and after storage at room temperature. Images for the RNA rings and filaments were similar and the PLI results are similar both room temperature and 4°C storage. In Figures 9 and 10, the images at left are unpolarized light images of the droplets. These images provide a detailed view of the droplet after LAD processing and storage. The wrinkled appearance in some figures is the result of water absorption at the surface of the drop. Wrinkling only occurred when droplets were moved from low RH environments into the higher RH of the room. When placed back in low RH wrinkling dissipated quickly. This effect was noted in previous studies and does not adversely affect the matrix or embedded biologic. ^[19]

The right panels of Figures 9 and 10 show the crossed-polarizer images of the samples. Regions of crystallization should appear as bright spots in these images. For these NANPs samples, no crystals were detected in the matrix immediately after LAD processing or after 1 of month storage. The LAD processed trehalose matrix was resistant to crystallization during processing and after storage at 4°C and at room temperature. In contrast, our previous studies using this PLI technique have demonstrated that air-dried samples do crystallize during low-humidity storage. ^[19] This is significant as crystallization of the matrix can damage embedded biologics.



(a) Before storage

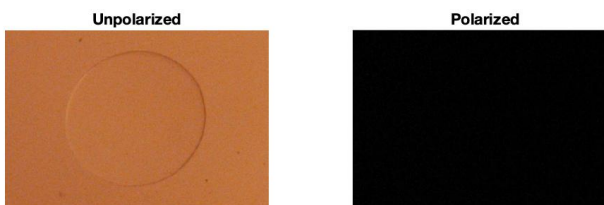


(b) After storage

Figure 9. Unpolarized and polarized images of DNA cubes LAD processed sample pre- and post-storage at 4°C.



(a) Before storage



(b) After storage

Figure 10. Unpolarized and polarized images of RNA cubes LAD processed sample pre- and post-storage at room temperature.

The amount of crystallization in droplets was characterized by determining a pixel area in each cross-polarizer image that was brighter than the background. Tables 2 shows the average crystal area after 1-month storage at 4°C. Table 3 displays the average crystal area at room temperature. The change in the crystal area is also shown in these tables. The average crystal area of all NANPs both before and after storage is small. There are some negative crystal growths for both storage at 4°C and at room temperature. There was no real decrease in crystal area in these samples. It is likely that the small errors in the selection of the background threshold brightness. Differences in the background brightness are due to small differences in the ambient lighting environment when unpolarized and polarized pictures of NANPs were taken.

Table 2. Average crystal growth of NANPs after 1-month storage at 4°C.

NANP name	Average crystalized area before storage (pixels)	Average crystalized area after storage (pixels)	Average crystal growth (pixels)
DNA cube	90 ± 60	30 ± 20	-60 ± 40
RNA cube	20 ± 10	30 ± 60	10 ± 10
RNA fiber	20 ± 20	16 ± 13	-10 ± 10
RNA ring	50 ± 40	70 ± 60	20 ± 20

Table 3. Average crystal growth of NANPs after 1-month storage at room temperature.

NANP name	Average crystalized area before storage (pixels)	Average crystalized area after storage (pixels)	Average crystal growth (pixels)
DNA cube	150 ± 120	120 ± 100	-30 ± 30
RNA cube	0 ± 0	0 ± 0	0 ± 0
RNA fiber	2 ± 1	0 ± 0	-2 ± 1
RNA ring	0 ± 0	10 ± 6	10 ± 6

3.3.2 LAD Processed RNA Rings Without Trehalose Added

Samples of RNA rings were also processed without trehalose to better understand the protective effect of this sugar. RNA rings (N=5) were processed for 30 minutes in the NANP

buffer solution (no trehalose buffer was added before processing). PLI was completed immediately after LAD processing (these samples were not stored). Figure 11 shows unpolarized (left) and polarized (right) images of the LAD processed RNA rings without trehalose. Notice that the sample appears as a dark patch in the unpolarized light image. The sample looks almost completely white in the polarized light image indicating there is a significant amount of crystallization in the sample. On average, the crystal area in the samples processed without trehalose was 12000 ± 3000 pixels, much higher than samples that contained trehalose. This is not surprising, as trehalose is the component of the preservation solution that can form an amorphous solid at room temperature. Without the trehalose, the sample is not amorphous and the salts in the buffer form a crystallization structure upon evaporation of the water in the solution.



Figure 11. Unpolarized and polarized images of LAD processed RNA rings without trehalose.

3.4 Gel Electrophoresis

3.4.1 DNA Cubes, RNA Cubes and RNA Rings

Figures 12-14 show the native-PAGE results for LAD processed DNA cubes, RNA cubes and DNA cubes, respectively. Each gel contains three sets of samples. From left to right for each sample set, the figures contain the results of an unprocessed control stored at 4 °C, a LAD processed sample stored at 4 °C, an unprocessed control stored at room temperature, and a LAD processed sample stored at room temperature. The controls were NANPs suspended in the LAD processing buffer containing trehalose. All native-PAGE results are free of stray fragments and

all bands are uniform. This indicates that the main structures of the DNA cubes, RNA cubes and RNA rings were not damaged significantly after LAD processing and being stored at 4 °C or at room temperature for 1 month.

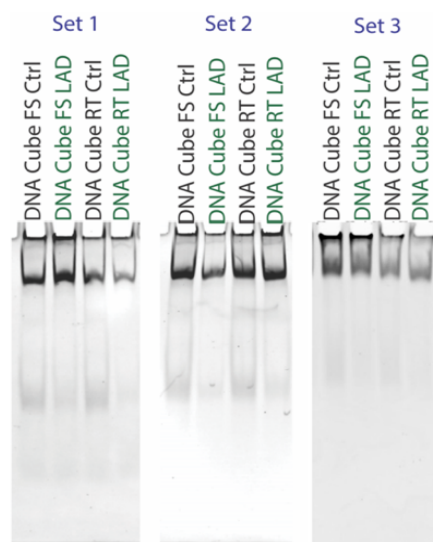


Figure 12. Native-PAGE visualizations of DNA cubes after 1 month of storage.

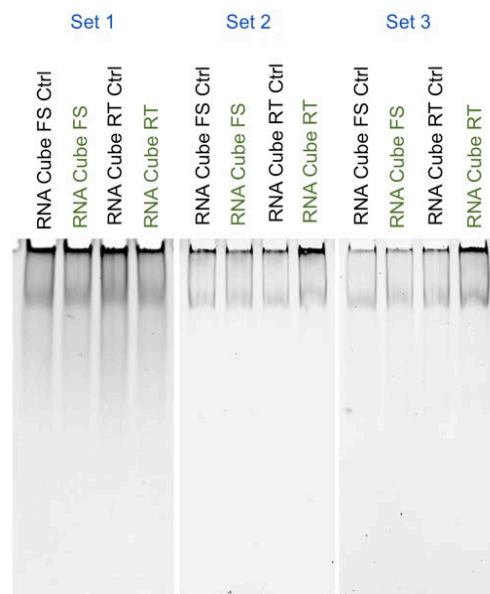


Figure 13. Native-PAGE visualizations of RNA cubes after 1 month of storage.

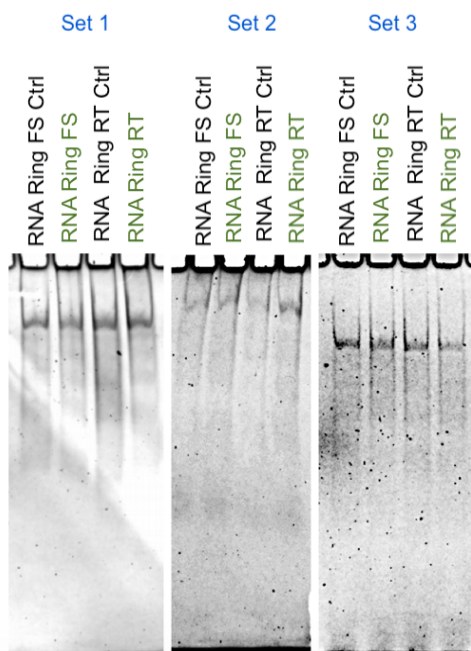


Figure 14. Native-PAGE visualizations of RNA rings after 1 month of storage.

3.4.2 RNA Fibers

Figure 15 shows the results of native-PAGE visualizations of RNA fibers. Each gel contains three sets of samples. From left to right for each sample, the figures contain the results of an unprocessed control stored at 4 °C, a LAD processed sample stored at 4 °C, an unprocessed control stored at room temperature, and a LAD processed sample stored at room temperature. No bands are evident in these images. The RNA fibers exhibit a range of sizes and this method is not ideal for detecting these particles. A different approach is required to detect changes to the structure of the RNA fibers.

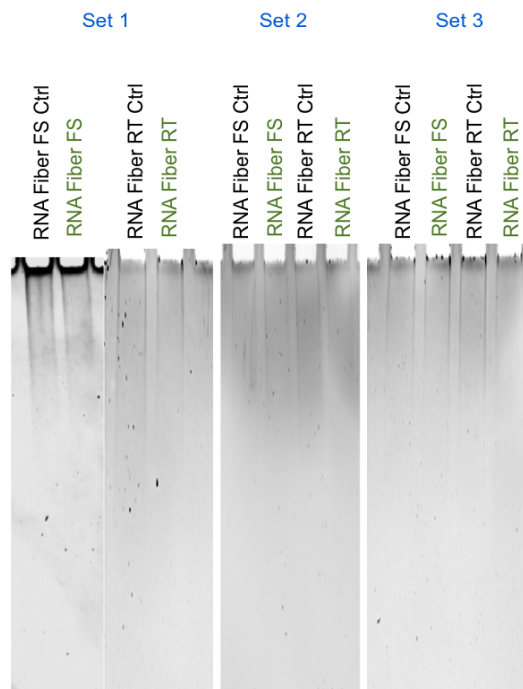


Figure 15. Native-PAGE visualizations of RNA fibers after 1 month of storage.

3.4.3. Storage With and Without Trehalose in a Liquid Buffer

To explore the effect of trehalose in stabilizing the NANPs without the LAD process, RNA cubes and RNA rings were stored for 24 days at 4°C and at room temperature both with and without trehalose added to the buffer (no LAD processing). Figure 16 shows the gel results with and without trehalose. The native-PAGE visualizations (see Figure 16) do not show stray fragments and exhibit consistent bands. This suggests that the NANPs are stable at 4°C and room temperature with and without trehalose added to the liquid buffer.

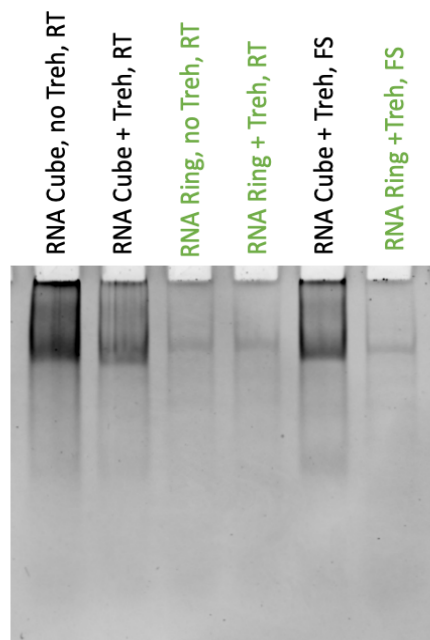


Figure 16. Native-PAGE visualizations of no-LAD RNA cubes and RNA rings after 24 days of storage.

3.4.4. LAD Processing Without Trehalose

Samples of RNA rings were LAD processed without the addition of trehalose to the buffer. These samples were not stored. Gels were completed immediately after LAD processing. As seen in section 3.3, this resulted in a dried product that was composed of crystalized buffer salts. Figure 17 shows the results of native-PAGE visualizations of these samples after LAD processing without trehalose, plus an unprocessed control stored at 4°C. All bands are uniform and there are no stray fragments. This indicates that without trehalose added after 30-minute LAD processing, the RNA ring particles are not degraded.

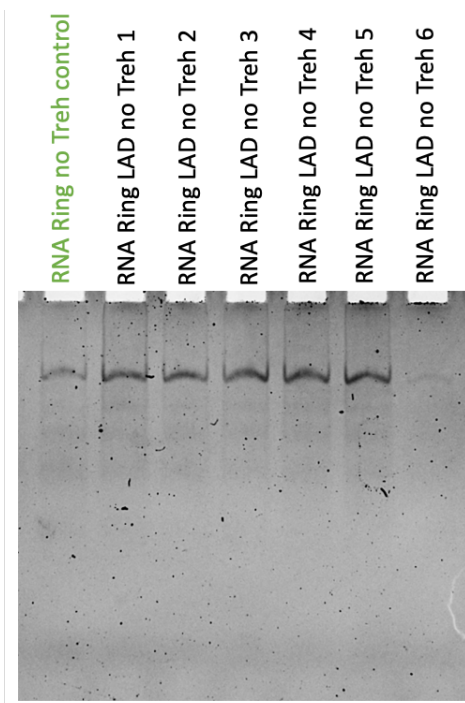


Figure 17. Native-PAGE gel of LAD processed RNA rings without trehalose and their control.

CHAPTER 4: DISCUSSION

From the drying curves and thermal histories of all 4 NANPs, a processing time of 30 minutes at 5 W for RNA NANPs and 4W for DNA cubes is sufficient to dehydrate the embedded biologics without causing any thermal damage. Using the thermal histories in conjunction with the drying curves allows for a determination of the optimum processing time for samples (i.e. reaching low EMC in the shortest time possible). Both the drying curves and thermal histories show that a processing time of 30 minutes is sufficient for reaching a low EMC value. Processing beyond 30 minutes does not significantly reduce the EMC. PLI shows that the trehalose matrix is stable against crystallization for all NANPs when stored at room temperature and 4°C for 1 month. Gel electrophoresis shows that RNA cubes, RNA rings, and DNA cubes in trehalose buffer are not damaged after 40 minutes of LAD processing and 1-month storage (at 4°C and at room temperature). Gel electrophoresis yielded inconclusive results for the RNA fibers.

Native-PAGE visualizations for NANPs stored at 4°C and room temperature in liquid buffers (no LAD processing) for 24 days indicate that the particles are stable in either buffer. The addition of trehalose does not seem to enhance the stability of these particles. LAD processing of RNA rings without trehalose also resulted in undamaged NANPs despite a large area of crystallization in the sample. Initial LAD experiments did show that the DNA cubes were damaged when processed at 5 W. This damage was prevented when the power was reduced to 4W, thus reducing the maximum temperature that the samples reached during processing. These results suggest that the NANPs can suffer thermal damage during processing but are less sensitive to mechanical stress of storage in a crystalline matrix.

For future work, LAD processed samples should be stored for extended times and at different temperatures with and without trehalose to better understand how robust NANPs can be

with and without trehalose. Further, more experiments need to be done to compare air drying to LAD processing with and without trehalose to examine whether rapid drying by laser is important in the stabilization of NANPs. Moreover, different techniques such as DSC, AFM, and/or Raman should be considered to better understand the structure and functionality of LAD processed samples. Also, Karl Fischer titration should be examined to achieve a more accurate end moisture content.

REFERENCES

- [1] Crowe, J. H. and Crowe, L. M., "Preservation of mammalian cells-learning nature's tricks," *Nat Biotechnol* **18**(2), 145–6 (2000).
- [2] Wolkers, W. F., Tablin, F., and Crowe, J. H., "From anhydrobiosis to freeze-drying of eukaryotic cells," *Comparative Biochemistry and Physiology a-Molecular & Integrative Physiology* **131**(3), 535–543 (2002).
- [3] Roy, I. and Gupta, M. N., "Freeze-drying of proteins: some emerging concerns," *Biotechnol Apply Biochem* **39**, 165–77 (2004).
- [4] Fonseca, F., Cenard, S., and Passot, S., "Freeze-drying of lactic acid bacteria," *Methods Mol Biol* **1257**, 477–88 (2015).
- [5] Wang, S., Goecke, T., and al., C. M., "Freeze-dried heart valve scaffolds," *Tissue Engineering Part C-Methods* **18**(7), 517–525 (2012).
- [6] Wang, S., Oldenhof, H., and al., T. G., "Sucrose diffusion in decellularized heart valves for freeze-drying," *Tissue Engineering Part C-Methods* **21**(9), 922–931 (2015).
- [7] Wang, W., "Lyophilization and development of solid protein pharmaceuticals," *International Journal of Pharmaceutics* **203**(1), 1–60 (2000).
- [8] Bjerketorp, J., Hakansson, S., and al., S. B., "Advances in preservation methods: keeping biosensor mi-croorganisms alive and active," *Curr Opin Biotechnol* **17**(1), 43–9 (2006).
- [9] Adams, G. D., "Lyophilization of vaccines: current trends," *Methods Mol Med* **87**, 223–44 (2003).
- [10] Chang, L., Shepherd, D., and al., J. S., "Mechanism of protein stabilization by sugars during freeze? Drying and storage: Native structure preservation, specific interaction,

- and/or immobilization in a glassy matrix?” *Journal of pharmaceutical sciences* **94**(7), 1427–1444 (2005).
- [11] Cicerone, M. T., Pikal, M. J., and Qian, K. K., “Stabilization of proteins in solid form,” *Adv Drug Deliv Rev* **93**, 14–24 (2015).
- [12] “Vacuum-Foam Drying: The Alternative for Lyophilization of Biologics?” *Lyophilizationworld* (2020).
- [13] R. D. Jangle, S. S. Pisal. “Vacuum Foam Drying: An Alternative to Lyophilization for Biomolecule Preservation.” *Indian Journal of Pharmaceutical Sciences* **74**(2), 91-100.
- [14] Millqvist-Fureby, A., Malmsten, M., and Bergenstahl, B., “Spray-drying of trypsin – surface characterization and activity preservation,” *International Journal of Pharmaceutics* **188**(2), 243-253 (1999).
- [15] Chakraborty, N., Menze, M. A., and al., H. E., “Trehalose transporter from african chironomid larvae improves desiccation tolerance of chinese hamster ovary cells,” *Cryobiology* **64**(2), 91–96 (2012).
- [16] Elmoazzen, H. Y., Lee, G. Y., and al., M. W. L., “Further optimization of mouse spermatozoa evaporative drying techniques,” *Cryobiology* **59**(1), 113–115 (2009).
- [17] Cellemme, S. L., Vorst, M. V., and al., E. P., “Advancing microwave technology for dehydration processing of biologics,” *Biopreserv Biobank* **11**(5), 278–84 (2013).
- [18] Young, M. A., Antczak, A. T., and al., A. W., “Light-assisted drying for protein stabilization,” *Journal of Biomedical Optics* **23**, 7 (2018).
- [19] Young, M. A., Furr, D. P., and al., R. Q. M., “Light-assisted drying for anhydrous preservation of biological samples: optical characterization of the trehalose preservation matrix,” *Biomedical Optics Express* **11**(2), 801–816 (2020).

- [20] Crowe, John H., L.M. Crowe, J.F. Carpenter and C. Aurell Wistrom. "Stabilization of dry phospholipid bilayers and proteins by sugars." *Biochemical Journal* **242.1**, 1, (1987).
- [21] Crowe, John H., Folkert A. Hoekstra, and Lois M. Crowe. "Anhydrobiosis." *Annual Review of Physiology* **54**, 579-599, (1992).
- [22] Israeli, Eitan, Brenda T. Shaffer, and Bruce Lighthart. "Protection of freeze-dried *Escherichia coli* by trehalose upon exposure to environmental conditions." *Cryobiology* **30.5**, 519-523, (1993).
- [23] Leslie, Samuel B., Eitan Israeli, B. Lighthart, John Crowe and L.M. Crowe. "Trehalose and sucrose protect both membranes and proteins in intact bacteria during drying." *Applied and environmental microbiology* **61.10**, 3592-3597, (1995).
- [24] Bieganski, Robert M., Alex Fowler, Jeffrey R. Morgan and Mehmet Toner. "Stabilization of active recombinant retroviruses in an amorphous dry state with trehalose." *Biotechnology progress* **14.4**, 615-620, (1998).
- [25] Wolkers, Willem F., Naomi J. Walker, Fern Tablin and John H. Crowe. "Human platelets loaded with trehalose survive freeze-drying." *Cryobiology* **42.2**, 79-87, (2001).
- [26] Chakraborty, Nilay, Michael A. Menze, Heidi Elmoazzen, Halong Vu, Martin L. Yarmush, Steven C. Hand and Mehmet Toner. "Trehalose transporter from African chironomid larvae improves desiccation tolerance of Chinese hamster ovary cells." *Cryobiology* **64**, 91-96, (2012).
- [27] Champion, D., Meste, M. L., and Simatos, D., "Towards an improved understanding of glass transition and relaxations in foods: molecular mobility in the glass transition range," *Trends in Food Science & Technology* **11**(2), 41–55 (2000).

- [28] Johnson MB, Chandler M, and Afonin KA., “Nucleic Acid Nanoparticles (NANPs) as Molecular Tools to Direct Desirable and Avoid Undesirable Immunological Effects,” *Advanced Drug Delivery Reviews* (2021).
- [29] Afonin KA*, Dobrovolskaia MA, Church G, and Bathe M*., “Opportunities, Barriers, and a Strategy for Overcoming Translational Challenges to Therapeutic Nucleic Acid Nanotechnology,” *ACS Nano* **14**(8), 9221-9227 (2020).
- [30] Chandler M, Panigaj M, Rolband LA, and Afonin KA., “Challenges to optimizing RNA nanostructures for large scale production and controlled therapeutic properties,” *Nanomedicine* **15**(19), 1915 (2020).
- [31] Panigaj M, Johnson MB, Ke W, McMillan J, Goncharova EA, Chandler M, and Afonin KA., “Aptamers as Modular Components of Therapeutic Nucleic Acid Nanotechnology,” *ACS Nano* **13**(11), 12301-12321 (2019).
- [32] Afonin KA, Kasprzak WK, Bindewald E, Kireeva M, Viard M, Kashlev M, Shapiro B., “*In silico* design and enzymatic synthesis of functional RNA nanoparticles,” *Accounts of Chemical Research* **47**(6), 1731–1741 (2014).
- [33] Rose, S. D., Kim, D.-H., and al., M. A., “Functional polarity is introduced by dicer processing of short substrate rnas,” *Nucleic acids research* **33**(13), 4140–4156 (2005).
- [34] Guo, P., “The emerging field of rna nanotechnology,” *Nature nanotechnology* **5**(12), 833–842 (2010).
- [35] Gross, M., “Dna nanotechnology gets real,” *Current biology: CB***23**(3), R95–98 (2013).
- [36] Afonin, K. A., Lindsay, B., and Shapiro, B. A., “Engineered rna nano designs for applications in rna nano-technology,” *DNA and RNA Nanotechnology* **1**, 1 (2013).
- [37] Mohri, K., Nishikawa, M., and al., Y. T., “Dna nanotechnology-based development of delivery systems for bioactive compounds,” *European Journal of Pharmaceutical*

- Sciences: Official Journal of the European Federation for Pharmaceutical Sciences* **58**, 26–33 (2014).
- [38] Kumar, V., Palazzolo, S., and al., S. B., “Dna nanotechnology for cancer therapy,” *Theranostics* **6**(5), 710–25 (2016).
- [39] Jasinski, D., Haque, F., and al., D. W. B., “The Advancement of the Emerging Field of RNA Nanotechnology”, *ACS Nano* (2017).
- [40] Furr, D., Lam, P. A., and Tran, A., “Thermal stabilization of nucleic acid nanoparticles (NANPs) using light-assisted drying,” SPIE (2021).
- [41] Afonin KA, Bindewald E, Yaghoubian AJ, Voss N, Jacovetty E, Shapiro BA, and Jaeger L., “*In vitro* assembly of cubic RNA-based scaffolds designed *in silico*,” *Nature Nanotechnology* **5**(9), 676-682 (2010).
- [42] Hong E, Halman J, Shah A, Khisamutdinov EF, Dobrovolskaia MA, Afonin KA., “Structure and composition define immunorecognition of nucleic acid nanoparticles,” *Nano Letters* **18**(7), 4309-4321 (2018).
- [43] Halman JR, Satterwhite E, Roark B, Chandler M, Viard M, Ivanina A, Bindewald E, Kasprzak WK, Panigaj M, Bui MN, Lu JS, Miller J, Khisamutdinov EF, Shapiro BA, Dobrovolskaia MA, Afonin KA., “Functionally-interdependent shape-switching nanoparticles with controllable properties,” *Nucleic Acids Research* **45**(4), 2210-2220 (2017).
- [44] Afonin KA, Kasprzak WK, Bindewald E, Puppala PS, Diehl ER, Kim TJ, Zimmermann MT, Jernigan RL, Jaeger L, Shapiro BA., “Computational and experimental characterization of RNA cubic nanoscaffolds,” *Methods* **67**(2), 256-265 (2013).
- [45] Afonin KA, Viard M, Kagiampakis I, Case C, Dobrovolskaia M, Hofmann J, Vrzak A, Kireeva M, Kasprzak WK, KewalRamani VN, Shapiro BA., “Triggering of RNA

- interference with RNA-RNA, RNA-DNA and DNA-DNA nanoparticles,” *ACS Nano* **9**(1), 251-259 (2015).
- [46] Rackley L, Stewart JM, Salotti J, Krokhotin A, Shah A, Halman JR, Juneja R, Smollett J, Lee L, Roark K, Viard M, Tarannum M, Vivero-Escoto J, Johnson PF, Dobrovolskaia MA, Dokholyan NV, Franco E, Afonin KA., “RNA fibers as optimized nanoscaffolds for siRNA coordination and reduced immunological recognition,” *Advanced Functional Material* **28**, 1805959 (2018).
- [47] Ke W, Hong E, Saito RF, Rangel MC, Wang J, Viard M, Richardson M, Khisamutdinov EF, Panigaj M, Dokholyan NV, Chammas R, Dobrovolskaia MA, Afonin KA., “RNA-DNA fibers and polygons with controlled immunorecognition activate RNAi, FRET, and transcriptional regulation of NF- κ B in human cells,” *Nucleic Acids Research* **47**(3), 1350-1361 (2019).
- [48] Halman JR, Kim KT, Gawk SJ, Pace R, Johnson MB, Chandler MR, Rackley L, Viard M, Marriott I, Lee JS, and Afonin KA., “A cationic amphiphilic co-polymer as a carrier of nucleic acid nanoparticles (NANPs) for controlled gene silencing, immunostimulation, and biodistribution,” *Nanomedicine: Nanotechnology, Biology and Medicine* **23**, 102094 (2020).
- [49] Juneja R#, Vadarevu H#, Halman J#, Tarannum M, Rackley L, Dobbs J, Marquez J, Chandler M, Afonin KA*, and Vivero-Escoto JL*., “Combination of Nucleic Acid and Mesoporous Silica Nanoparticles: Optimization and Therapeutic Performance In Vitro,” *ACS Applied Materials & Interfaces* (2020).
- [50] Grabow WW, Zakversky P, Afonin KA, Chworos A, Shapiro BA, Jaeger L., “Self-assembling RNA nanorings based on RNAI/II inverse kissing complexes,” *Nano Letters* **11**(2), 878-887 (2011).

- [51] Afonin KA, Grabow WW, Walker FM, Bindewald E, Dobrovolskaia MA, Shapiro BA, Jaeger L., “Design and self-assembly of siRNA-functionalized RNA nanoparticles for use in automated nanomedicine,” *Nature Protocols* **6**(12), 2022-2034 (2011).
- [52] Afonin KA, Kireeva M, Grabow WW, Kashlev M, Jaeger L, Shapiro BA., “Co-transcriptional assembly of chemically modified RNA nanoparticles functionalized with siRNAs,” *Nano Letters* **12**(10), 5192-5195 (2012).
- [53] Afonin KA, Viard M, Koyfman AY, Martins AN, Kasprzak WK, Panigaj M, Desai R, Santhanam A, Grabow WW, Jaeger L, Heldman E, Reiser J, Chiu W, Freed EO, Shapiro BA., “Multifunctional RNA nanoparticles,” *Nano Letters* **14**(10), 5662-5671 (2014).
- [54] Afonin KA*, Viard M, Tedbury P, Bindewald E, Parlea L, Howington M, Valdman M, Johns-Boehme A, Brainerd C, Freed EO, Shapiro BA*., “The use of minimal RNA toeholds to trigger the activation of multiple functionalities,” *Nano Letters* **16**(3), 1746-1753 (2016).
- [55] Sajja S#, Chandler M#, Federov D, Kasprzak WK, Lushnikov AY, Viard M, Shah A, Dang D, Dahl J, Worku B, Dobrovolskaia MA, Krasnoslobodtsev A, Shapiro BA, Afonin KA., “Dynamic behavior of RNA nanoparticles analyzed by AFM on a mica/air interface,” *Langmuir* **34**(49), 15099-15108 (2018).

* – corresponding authors

– equal contribution